

Excitation of low- n TAE instabilities by energetic particles in global gyrokinetic tokamak plasmas

Y. Nishimura *

Plasma and Space Science Center, National Cheng Kung University, Tainan 70101, Taiwan

Abstract

The first linear global electromagnetic gyrokinetic particle simulation on the excitation of toroidicity induced Alfvén eigenmode (TAE) by energetic particles is reported. With an increase in the energetic particle pressure, the TAE frequency moves down into the lower continuum.

PACS numbers: 52.55.Fa, 52.35.Bj, 52.65.Tt

Toroidicity induced Alfvén eigenmode (TAE)¹⁻³ can play important roles in burning plasmas. The TAE modes can be excited when energetic particles, for example fusion born alpha particles, resonate with the phase velocity of the shear Alfvén wave which resides within the frequency gap of the Alfvén continuum.

Shear Alfvén wave oscillations, continuum damping, and the appearance of the frequency gap in toroidal geometries by gyrokinetic particle simulation have been recently reported.⁴ The simulation of Ref.4 is demonstrated in the long wavelength magnetohydrodynamic (MHD) like limit in the absence of kinetic ions. In this letter, taking exactly the same parameters^{3,4} but adding the energetic ion particles, the first linear particle simulation on the excitation of the TAE modes is reported. The simulation is done without employing

*Previous address : Department of Physics and Astronomy, University of California, Irvine, California 92697, USA

MHD equation. The simulation is not the conventional gyrokinetic-MHD hybrid ones,⁵⁻⁷ where the kinetic ions enter the system through the stress tensor. The setting of the simulation is kept as faithful as possible to Ref.3 and 4 to see an explicit connection with our previous studies.⁴

A simplified linearized set of equations is employed⁸ for the numerical simulation which is reduced from the electron-fluid ion-kinetic hybrid gyrokinetic model.⁹⁻¹² The equations of Ref.4 are normalized by the ion Larmor radius (at the electron temperature) for the length, the ion cyclotron frequency for time, and the electron temperature for the electrostatic potential, and the magnetic field strength at the magnetic axis, B_0 . The set of the equations are the electron continuity equation

$$\frac{\partial \delta n_e}{\partial t} = -\nabla_{\parallel} \delta u_{\parallel e} \quad (1)$$

(δn_e is the fluid electron density and $\delta u_{\parallel e}$ is parallel electron velocity), the inverse of Faraday's law

$$\frac{\partial A_{\parallel}}{\partial t} = \nabla_{\parallel} (\Phi_{eff} - \Phi) \quad (2)$$

(A_{\parallel} is the vector potential, Φ is the electrostatic potential, and Φ_{eff} is the effective potential representing the total parallel electric field), the gyrokinetic Poisson equation¹³

$$\Phi - \tilde{\Phi} = \delta \bar{n}_{\alpha} - \delta n_e \quad (3)$$

($\delta \bar{n}_{\alpha}$ is the gyro-averaged energetic particle density, $\tilde{\Phi}$ is the second gyrophase averaged electrostatic potential¹³) the lowest order adiabatic relation

$$\Phi_{eff} = \delta n_e, \quad (4)$$

and the inverse of Ampere's law

$$\delta u_{\parallel e} = \beta_e^{-1} \nabla_{\perp}^2 A_{\parallel} + \delta u_{\parallel \alpha}. \quad (5)$$

The parallel velocity of the energetic particles is given by $\delta u_{\parallel \alpha}$. Here $\beta_e = (c_s/v_A)^2$ where c_s is the sound velocity and v_A is the Alfvén velocity. All the variables in Eqs.(1)-(5) are the

normalized ones. The gradient operators ∇_{\perp} and ∇_{\parallel} are those in the direction perpendicular and parallel to the equilibrium magnetic field.

By coupling Eqs.(1)-(5), the shear Alfvén wave dispersion relation in the toroidal geometry, Eq.(2) of Ref.3 can be obtained. Figure 1 shows the shear Alfvén wave frequency as a function of the radial coordinate r (a is the minor radius), which is equivalent to Fig.1 of Ref.3. Due to the $1/R$ variation of the toroidal magnetic field (R is the major radius), the cylindrical Alfvén continuum (dashed lines) breaks up and the frequency gap (or the frequency forbidden band) appears within the range of $0.299 < \omega/\omega_A < 0.389$. Here, ω_A is the Alfvén frequency at the magnetic axis.

Equations (1)-(5) are employed (with the $\delta\bar{n}_{\alpha}$ and $\delta u_{\parallel\alpha}$ terms *turned off*) in the simulation of Fig. 5 of Ref. 4. On top of Eqs.(1)-(5) we add kinetic ions. The guiding center equation and the δf gyrokinetic equation (the weight equation)¹⁴ are solved for the kinetic energetic particle ions (we neglect thermal kinetic ions, however). Taking the perturbed distribution function δf_{α} , the energetic particle density (velocity) in Eq.3 [Eq.(5)] is given by $\delta\bar{n}_{\alpha} = r_{\alpha} \int \delta f_{\alpha} d^3v$ ($\delta u_{\parallel\alpha} = r_{\alpha} \int v_{\parallel} \delta f_{\alpha} d^3v$), where $\int d^3v$ is an average over the velocity space. Note that in the simulation, we control the perturbed density of the energetic particles by multiplying a factor r_{α} ($r_{\alpha} < 1$) which is proportional to the equilibrium energetic particle density. The energetic ion particles are provided with the Maxwellian distribution function $f_{0\alpha} \propto \exp(-v_{\parallel}^2/2v_{\alpha}^2)$ in the velocity space (thus $\partial f_{0\alpha}/\partial v_{\parallel}$ is always negative).¹⁵ The resonating energetic particles are *inserted* within the frequency gap by utilizing a portion of the Maxwellian distribution function whose thermal velocity is of the order of Alfvén speed.

The particles that resonate with the shear Alfvén wave with the phase velocity ω/k_{\parallel} can destabilize the TAE mode, when the mode frequency ω is within the frequency gap (we choose $\omega/\omega_A = 0.344$ in the middle of the gap in Fig.1), and when the parallel wave vector $k_{\parallel} = (m - nq)/qR$ satisfies $k_{\parallel} = -k_{\parallel m} = k_{\parallel m+1}$ at $q = (2m + 1)/2n$. Here, m (n) stands for the poloidal (toroidal) mode number. We take $m = 1$, $m + 1 = 2$, and $n = 1$ which is equivalent to $m = -2$, $m + 1 = -1$, and $n = -1$ of Ref.3. The geometrical parameters used for the simulation are the same as in Refs.3 and 4 (for example, the inverse aspect ratio of

0.375 and a parabolic safety factor q). The major radius is given by $R = 46.6\text{cm}$ as well (after convincing the TAE excitation in the originally published setting,⁴ we move on to a parameter survey in a larger size plasma). From the ω and the k_{\parallel} values chosen above, we provide the Maxwellian distribution with $v_{\alpha} = \omega/k_{\parallel} = 10.32c_s$. The mass and the charge of the energetic particles are that of the Hydrogen ion. In the specific simulation below, we set $\beta_e = 0.01$, and the constant density gradient $\kappa_n = -R(1/n_{\alpha})(dn_{\alpha}/dr) = 8.0$. Here, n_{α} represents the equilibrium density of the energetic particles. The temperature gradient parameters⁴ are set to be zero. In Eq.(3) and Eq.(5), $r_{\alpha} = 0.15$ is taken for Figs.2 and 3.

The simulation is conducted by an electromagnetic extension⁴ of the GTC code^{16–18} with a non-iterative field solver.^{19,20} With the additional energetic particle drive, the TAE mode is excited. A linear eigenmode (contour plot) of the TAE instability is shown in Fig.2. Note that the contour plots are not up-down symmetric due to the finite poloidal shear flow.²¹

The frequency spectrum of the TAE instability is shown in Fig.3. The TAE frequency ($\omega/\omega_A = -0.36$) is found within the gap (and not on the gap boundaries as in Ref.4)²² which is a clear evidence of the TAE excitation. The linear growth rate of the TAE instability is given by $\gamma/\omega_A = 0.0215$ (and thus $|\gamma/\omega| = 6.0\%$) for both the $m = 1$ and $m = 2$ mode.

Figure 4 shows the linear TAE growth rates (divided by the real frequency) versus the multiplication factor r_{α} . Compared to the calculations in Figs.2 and 3, a twice larger plasma size is taken for Fig.4 (the Larmor radius of the energetic particles in Figs.2 and 3 are 15% of the minor radius while 7.5% in Fig.4). We see a monotonic increase in the growth rate as the energetic particle population increase (and thus the effective beta value of the energetic particles, β_{α} increases; at $\beta_e = 0.01$, a simple estimate will give $\beta_{\alpha} = 4\pi n_{\alpha}T_{\alpha}/B_0^2 \sim r_{\alpha}$. Here T_{α} is the energetic particle temperature). On the other hand, the real frequency of the mode decreases (approximately 15% of a reduction in the real frequency) as r_{α} (or β_{α}) increases and crosses the lower gap boundary²³ (but not the upper gap boundary) which is suggested by the analysis in Ref.24 (Resonant TAE, which emphasizes the resonance between the mode frequency and the magnetic drift frequency of the energetic particles).²⁴ As a reference, the energetic particle mode (EPM)²⁵ refers to a heating of the continuum based on the notion

that the energetic particle drive exceeds the continuum damping and predicts the appearance of the mode frequency both in the upper and the lower continuum. The square plots in Fig.4 represents the analysis of the TAE growth rate in a large aspect ratio tokamak from Ref.3 (the simulation results and the analysis compare favorably at higher β_α).

We note that instability growth was already minimal at $r_\alpha = 0.025$ (with the specific simulation parameters we employed in Fig.4), and we did not survey below $r_\alpha < 0.025$ in this work. The TAE mode in its nature should not have an instability threshold. The latter onset feature needs to be investigated in detail to see the limitation of the initial value approach (if any). We also would like to remind that a simplified model Eqs.(1)-(5) is employed in this letter (so as to primary focus on the excitation of TAE by the additional energetic particles).⁴ The radial extension of the simulation domain is limited to $0.1 < r/a < 0.9$ (see Fig.2). An inclusion of the magnetic axis can be crucial to describe the long wavelength global modes precisely.

In summary, the first linear excitation of the low-n TAE modes by the energetic particles in a global gyrokinetic particle simulation is reported.²⁶ The work did not employ MHD model (through closure relations). With a completion of the current global gyrokinetic simulation method, one can investigate the onset and the saturation mechanism of the TAE modes simultaneously without any restrictions on the wavelength of the modes. Apparently, the advantage of initial value approach is its application for nonlinear simulation. We plan to report the analysis of energetic particles driven high-n Alfvénic modes separately. Whether which mode numbers are most unstable is a great interest to large tokamak burning plasma experiments.

The author would like to thank Dr. Z. Lin, Dr. W. X. Wang, Dr.P. H. Diamond, Dr. T. S. Hahm, Dr. B. Scott, Dr. M. Yagi, Dr.K. C. Shaing, and Dr. C. Z. Cheng for discussions. This work is supported by Department of Energy (DOE) SciDAC Center for Gyrokinetic Particle Simulation and National Cheng Kung University Top University Project. The simulation is done employing National Energy Research Scientific Computing Center (NERSC) supercomputers by the year 2007 during YN's residence at the University

of California, Irvine.

REFERENCES

1. C. Z. Cheng, L. Chen, and M. S. Chance, Ann. Phys. (N.Y.) **161**, 21 (1985).
2. C. Z. Cheng and M. S. Chance, Phys. Fluids **29**, 3695 (1986).
3. G. Y. Fu and J. W. Van Dam, Phys. Fluids B **1**, 1949 (1989).
4. Y. Nishimura, Z. Lin, and W. X. Wang, Phys. Plasmas **14**, 042503 (2007).
5. W. Park *et al.*, Phys. Fluids B **4**, 2033 (1992).
6. G. Y. Fu and W. Park, Phys. Rev. Lett. **74**, 1594 (1995).
7. C. Z. Cheng, J. Geophys. Res. **96**, 159 (1991).
8. These simplified equations are employed for the simulation of the Alfvén eigenmodes in Ref.4 (but not for the micro-instability part).
9. Y. Chen and S. Parker, Phys. Plasmas **8**, 441 (2001).
10. Z. Lin and L. Chen, Phys. Plasmas **8**, 1447 (2001).
11. W. X. Wang, L. Chen, and Z. Lin, Bull. Am. Phys. Soc. **46**, 114 (2001).
12. F. L. Hinton, M. N. Rosenbluth, and R. E. Waltz, Phys. Plasmas **10**, 168 (2003).
13. W. W. Lee, J. Comput. Phys. **72**, 243 (1987).
14. A. M. Dimits and W. W. Lee, J. Comput. Phys. **107**, 309 (1993).
15. M. N. Rosenbluth and P. H. Rutherford, Phys. Rev. Lett. **34**, 1428 (1975).
16. Z. Lin and W. W. Lee, Phys. Rev. E **52**, 5646 (1995).
17. R. B. White and M. S. Chance, Phys. Fluids **27**, 2455 (1984).
18. Z. Lin, T. S. Hahm, W. W. Lee, W. M. Tang, and R. B. White, Science **281**, 1835 (1998).

19. Y. Nishimura, Z. Lin, J. L. V. Lewandowski, and S. Ethier, *J. Comput. Phys.* **214**, 657 (2006).
20. Y. Nishimura and Z. Lin, *Contrib. Plasma Phys.* **46**, 551 (2006).
21. J. Y. Kim, Y. Kishimoto, M. Wakatani, and T. Tajima, *Phys. Plasmas* **3**, 3689 (1996).
22. We remind that the upper branch of the continuum accumulates more prominently than the lower branch as predicted at the zero resistivity limit of the periodic shear Alfvén wave mode.^{1,24} See Fig.5(b) of Ref.4.
23. N. N. Gorelenkov, C. Z. Cheng, and W. M. Tang, *Phys. Plasmas* **5**, 3389 (1998).
24. C. Z. Cheng, N. N. Gorelenkov, and C. T. Hsu, *Nucl. Fusion* **35**, 1639 (1995).
25. F. Zonca and L. Chen, *Phys. Plasmas* **3**, 323 (1996).
26. The TAE eigenmode structures by gyrokinetic particle simulation in the absence of energetic particles are exhibited in a very recent work by A. Mishchenko, R. Hatzky, and A. Könies, *Phys. Plasmas* **15**, 112106 (2008).

FIGURES

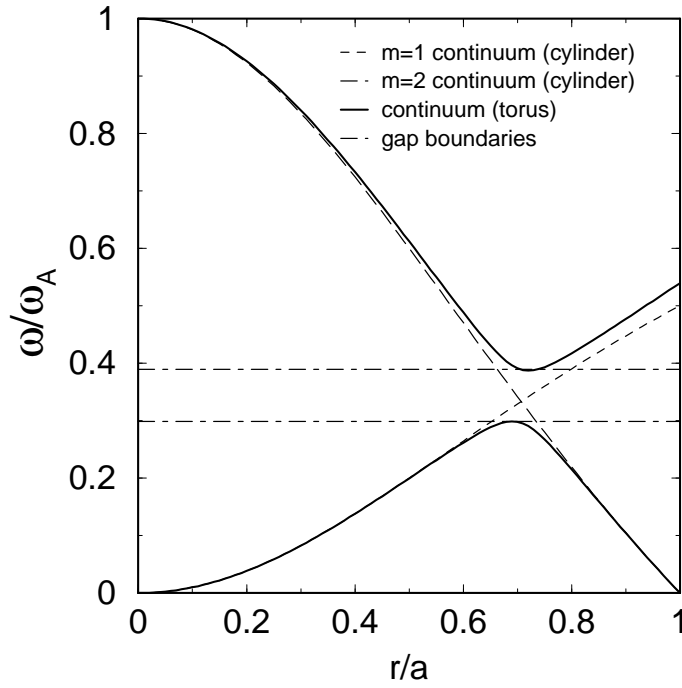


FIG. 1. Shear Alfvén frequency as a function of the radial location. The dashed curves are the continuum frequencies for the cylindrical limit, for $m = 1$ and $m = 2$ modes. The solid lines are for the continuum frequency with the toroidal geometry effect. The lower (upper) boundary of the upper (lower) curve is at $\omega/\omega_A = 0.389$ ($\omega/\omega_A = 0.299$). Correspondingly the frequency gap (the forbidden frequency range) appears within the range of $0.299 < \omega/\omega_A < 0.389$. The figure is a recapitulation of Fig.1 of Ref.3.

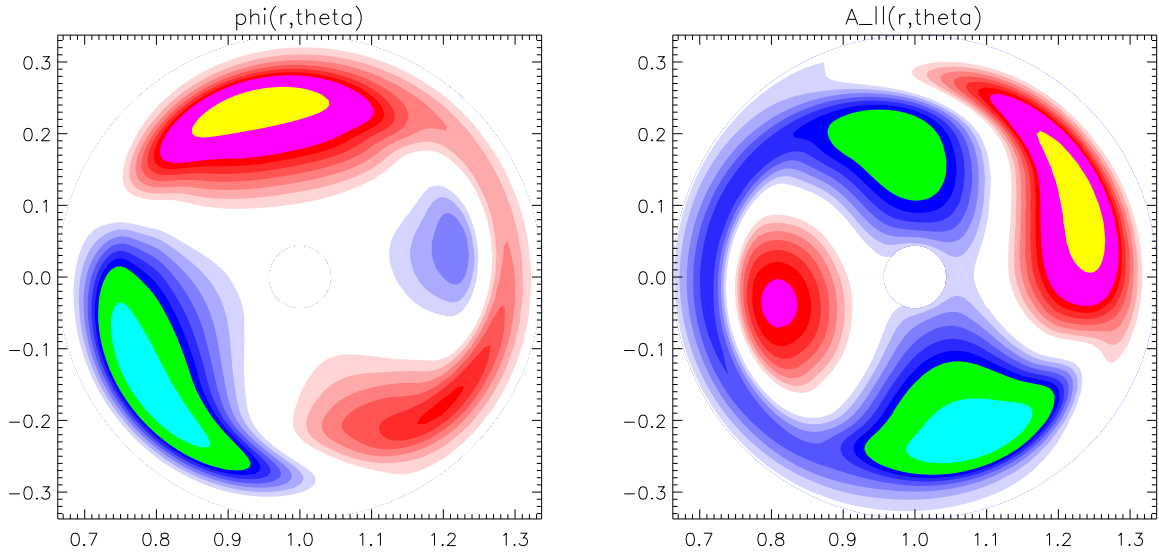


FIG. 2. (Color online) Linear eigenmodes (contour plots on a poloidal plane) of TAE instability. (a) The electrostatic potential Φ at a toroidal angle $\zeta = 0$. Red represents positive Φ values, while blue represents negative Φ values. (b) The vector potential A_{\parallel} at a toroidal angle $\zeta = 0$.

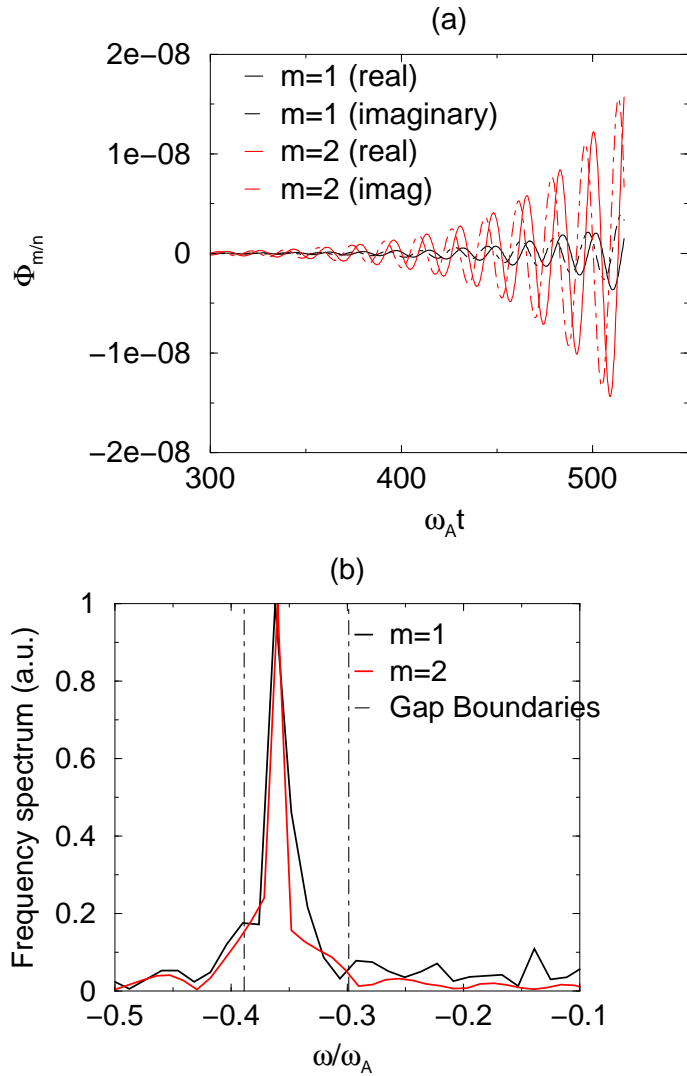


FIG. 3. (Color online) (a) The Fourier components of the electrostatic potential Φ as a function of time. (b) The frequency spectrum obtained from the time series of Fig.3(a) (black for $m = 1$, red for $m = 2$).

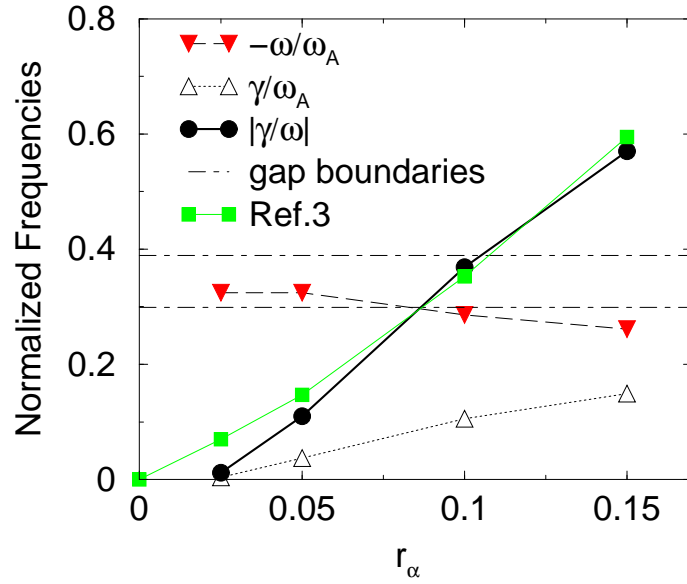


FIG. 4. (Color online) Dependence of the real frequency ω , and the linear growth rate γ on r_α (and thus β_a). For each data, eigenmode structures similar to Fig.2 are obtained. The green squares represent the analytical TAE growth rate - real frequency ratio in a large aspect ratio tokamak from Ref.3.